Technical Correspondence

3-D Palmprint Recognition With Joint Line and Orientation Features

Wei Li, David Zhang, Lei Zhang, Guangming Lu, and Jingqi Yan

Abstract—2-D palmprint has been recognized as an effective biometric identifier in the past decade. Recently, 3-D palmprint recognition was proposed to further improve the performance of palmprint systems. This paper presents a simple yet efficient scheme for 3-D palmprint recognition. After calculating and enhancing the mean-curvature image of the 3-D palmprint data, we extract both line and orientation features from it. The two types of features are then fused at either score level or feature level for the final 3-D palmprint recognition. The experiments on The Hong Kong Polytechnic University 3-D palmprint database, which contains 8000 samples from 400 palms show that the proposed feature extraction and fusion methods lead to promising performance.

Index Terms—3-D palmprint identification, biometrics, feature fusion, mean curvature.

I. INTRODUCTION

AUTOMATIC personal authentication using biometric characteristics plays a key role in applications of public security, access control, forensics, and e-banking, etc. Many kinds of biometric authentication techniques have been developed based on different biometric characteristics, such as fingerprint, face, iris, palmprint, and hand shape. 2-D palmprint recognition [1]–[4], [16]–[18] has been widely studied in the past decade and it has been proven that palmprint is a unique biometric identifier. 2-D palmprint systems have merits of high accuracy and user friendliness, etc. Nonetheless, 2-D palmprint can be easily counterfeited and much 3-D palm structural information is lost. Inspired by the success of 3-D techniques in biometric authentication, such as 3-D face [5] and 3-D ear recognition [6], very recently, a structured-light-imaging-based [7], [8] 3-D palmprint system [9] was developed to capture the depth information of palmprint. In [9], the mean curvature and Gaussian curvature are calculated from the depth information and they serve as the basic features for 3-D palmprint matching and recognition.

As shown in [9], the mean curvature is a stable and distinct feature of 3-D palmprint. By normalizing and mapping the mean-curvature values to a plane, we can get a mean-curvature image (MCI) that contains line structure features and texture features of the 3-D palmprint. In [9], the MCI was binarized to highlight the line features and the binarized MCI was used as the feature map for 3-D palmprint matching. However, the binarization operation loses much the texture information existing in the MCI. Actually, if we view the MCI of a 3-D palmprint as a 2-D palmprint image, then many 2-D palmprint feature-extraction techniques can be applied. In addition, the line and texture features could provide complementary information for palmprint discrimination. Therefore, in this paper, we propose to extract both line and texture features from MCI and fuse them efficiently for more accurate 3-D palmprint recognition.

There are two main approaches to 2-D palmprint recognition: line-based approach [16]–[18] and texture-based approach [2], [3]. For the representative line-based methods, Li *et al.* proposed a modified line-based Hausdorff distance for palmprint identification [16]; Wu *et al.* proposed a set of directional line detectors and used them to extract the palm lines for palmprint matching [17]; Huang *et al.* proposed a modified finite radon transform to extract the principal lines in palmprint [18]. With respect to the texture-based methods, the most representative one may be competitive coding (CompCode) scheme proposed by Kong *et al.* [2], where a series of directional Gabor filters were used to extract the orientation features of palmprint. Sun *et al.* proposed an ordinal palmprint representation for personal identification [3].

With the MCI of 3-D palmprint data, the line features can be easily extracted by setting a global threshold to segment the high curvature regions. For texture features, we can use six directional Gabor filters to extract the local orientation from the MCI, like what the CompCode method does on 2-D palmprint images [2]. In our preliminary study [19], the line and orientation features are directly extracted from the MCI and they are fused at matching score level. In this paper, we propose to use the Butterworth low-pass Filter (BLPF) to enhance the MCI before feature extraction, and fuse the extracted line and orientation features on the feature level. A series of experiments are conducted by using The Hong Kong Polytechnic University (HKPU) 3-D palmprint database, which contains 8000 samples collected from 400 palms. The experimental results show that the proposed method is very promising, outperforming significantly the methods in [9] and [19]. Particularly, the proposed feature-level fusion can not only achieve higher accuracy than the score level fusion presented in [19], but also require much less matching time.

The rest of the paper is organized as follows. Section II discusses the calculation of MCI. Section III introduces the line and orientation feature extraction. Section IV presents the matching and fusion scheme. Section V presents the experimental results and Section VI concludes the paper.

II. MCI PROCESSING

A. Region of Interest Extraction

In [9], we have developed a structured-light-imaging-based 3-D palmprint-acquisition device. The 3-D palmprint data are typical range data, which are represented by cloud points. Fig. 1(c) shows a 3-D palmprint sample (resolution: 768×576) collected by our device. For a better visualization of the 3-D palmprint, Fig. 1(c) is rendered by OpenGL. We can see that in the 3-D palmprint image, the cloud points in the boundary area and in the fingers are not suitable for feature

This article has been accepted for inclusion in a future issue of this journal. Content is final as presented, with the exception of pagination.

2   IEEE TRANSACTIONS ON SYSTEMS, MAN, AND CYBERNETICS—PART C: APPLICATIONS AND REVIEWS
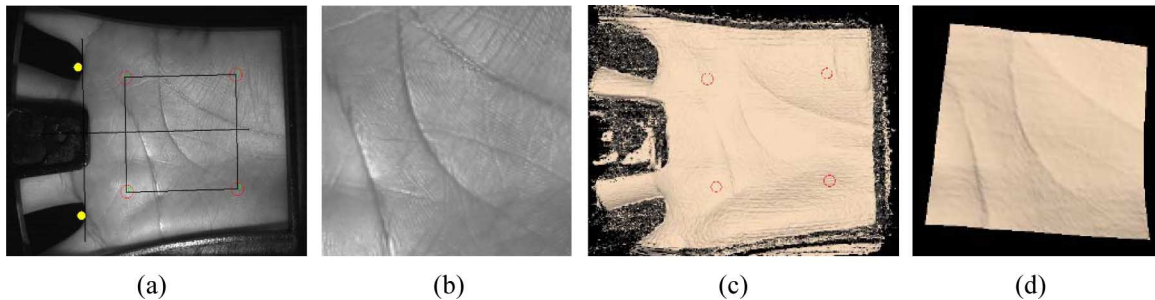

Fig. 1.   ROI extraction of 3-D palmprint from its 2-D counterpart. (a) 2-D palmprint image, adaptively established coordinate system, and ROI (i.e., the rectangle). (b) Extracted 2-D ROI. (c) 3-D palmprint image whose cloud points have a one-to-one correspondence to the pixels in the 2-D counterpart. (d) Obtained 3-D ROI by extracting the cloud points corresponding to the pixels in 2-D ROI.
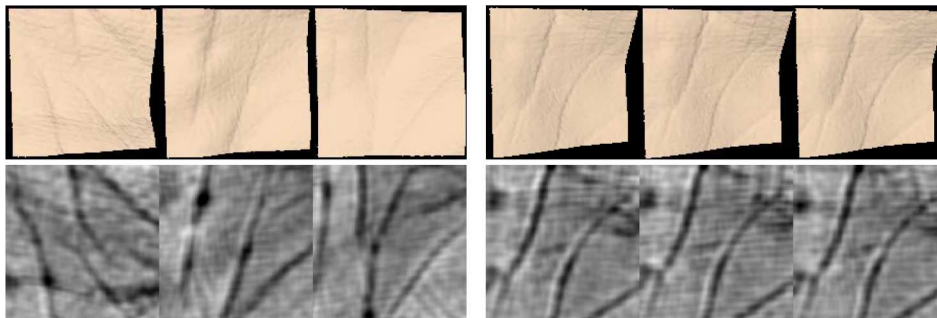

Fig. 2.   3-D ROI images (first row) and their MCI images (second row). The first three palmprint images are from different palms, while the last three palmprint images are from the same palm. (Please note that we change the viewpoint of 3-D ROI for better visualization.)

extraction and recognition. Most of the useful and stable features locate in the center area of the palm. In addition, at different times when the user puts his/her hand on the collecting device, there will be some relative displacements of the positions of palm, even that we impose some constraints on the users to place their hands. Therefore, before feature extraction, it is necessary to perform some preprocessing to align the palmprint and extract the central area of it, which is called the region of interest (ROI) extraction.

Our 3-D palmprint data-acquisition device can capture a 3-D palmprint image and a 2-D palmprint image simultaneously. As in [9], we extract the 3-D ROI with the aid of its corresponding 2-D counterpart. Fig. 1(a) shows a 2-D palmprint image, the established local coordinate system by using the algorithm in [1] and the ROI (i.e., the rectangle). Fig. 1(b) shows the extracted 256×256 2-D ROI. Because the points in 3-D palmprint image have a one-to-one correspondence to the points in its 2-D counterpart, we can easily obtain the 3-D ROI by extracting the cloud points corresponding to the 2-D ROI. Fig. 1(d) shows the extracted 3-D ROI from Fig. 1(c). (Note that we use a different viewpoint to show the 3-D ROI in Fig. 1(d).) By using the ROI extraction procedure, the 3-D palmprint images are aligned so that the small translation and rotation introduced in the data-acquisition process are corrected. In addition, the data amount used in the following feature extraction and matching process is significantly reduced. This will save much computational cost.

B. Curvature Calculation

With the ROI obtained from the original 3-D palmprint data, stable and unique features are expected to be extracted for the following pattern matching and recognition. The mean and Gaussian curvatures are intrinsic measures of a surface, i.e., they depend only on the surface shape, but not on the way, how the surface is placed in the 3-D space

[10]. Thus, such curvature features are robust to the rotation, translation, and even some deformation of the palm. From the study in [9], we know that the mean curvature is more informative than the Gaussian curvature in 3-D palmprint recognition. Thus, to save computation, we only consider the mean curvature in the following development. We adopt the algorithm in [11] to estimate the mean curvature from 3-D palmprint data for its simplicity and effectiveness as follows:

$$H = \frac{(1 + (h_y)^2)h_{xx} - 2h_x h_y h_{xy} + (1 + (h_x)^2)h_{yy}}{2(1 + (h_x)^2 + (h_y)^2)^{3/2}} \quad (1)$$

where h is the height of the points on the palmprint to the reference plane, h_x, h_y, h_{xx}, h_{yy}, and h_{xy} are the first, second, and hybrid partial derivatives of h to x- and y-coordinates separately.

With (1), the mean curvatures of a 3-D palmprint ROI can be calculated. For better visualization and more efficient computation, we convert the original curvature images into gray-level images with integer pixels. We first normalize the mean-curvature value H to $\bar{H}$ as follows:

$$\bar{H}(i, j) = 0.5(H(i, j) - \mu)/(4\delta) + 0.5 \quad (2)$$

where μ and δ are the mean and standard deviation of the curvature value. With (2), most of the curvature values will be normalized into the interval [0,1]. We then map $\bar{H}(i, j)$ to an 8-bits gray-level image $G(i, j)$ as follows:

$$G(i, j) = \begin{cases} 0, & \bar{H}(i, j) \leq 0 \\ \text{round}(255 \times \bar{H}(i, j)), & 0 < \bar{H}(i, j) < 1 \\ 255, & \bar{H}(i, j) \geq 1. \end{cases} \quad (3)$$

We call image $G(i, j)$ the MCI. Fig. 2 illustrates the MCI images from the same palm (at different times) and different palms. We can see that the 2-D MCI images can well preserve the 3-D palm surface features. Not only the principal lines, which are the most important

This article has been accepted for inclusion in a future issue of this journal. Content is final as presented, with the exception of pagination.

IEEE TRANSACTIONS ON SYSTEMS, MAN, AND CYBERNETICS—PART C: APPLICATIONS AND REVIEWS
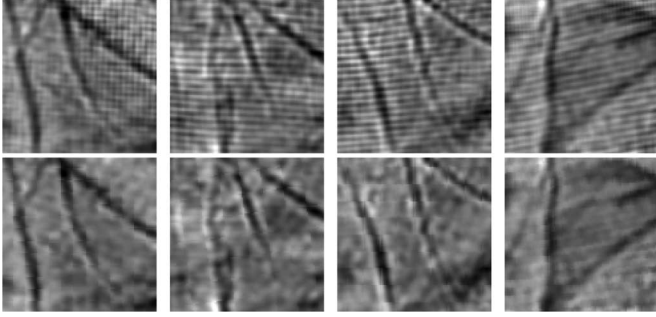
3

Fig. 3. Noise removal of MCI. The first row is the original MCI, and the second row is the MCI filtered by BLPF.

and stable features in palmprint recognition, are clearly enhanced in MCI, but also the depth information of different shape structures is well preserved.

C. Noise Removal

In the 3-D palmprint data-acquisition process, noise will be inevitably introduced. This can be clearly observed in the MCI images in Fig. 2. The noise mainly comes from two sources. One is the system electrical circuit hardware. Such system noise is often the mixture of high-frequency periodical noise and white noise. The other source is the imaging object, i.e., the palm. The palm is not a rigid object and its small deformations in the data-collection process add random noise to the collected data. It is necessary to remove noise from the raw MCI images for a robust feature extraction. Considering the fact that these noises will mainly fall into the high-frequency band, we simply use a BLPF [12] to reduce them. The BLPF is defined as

$$H(u,v) = \frac{1}{1 + [D(u,v)/D_0]^{2n}}, \quad u = 1, 2, \ldots, M,$$
$$v = 1, 2, \ldots, N \quad (4)$$

where $M*N$ is the image size, D_0 is the cut-off frequency (20 is used in our experiments), n is the order of BLPF and we set it to 4 by experience, and $D(u,v)$ is defined as

$$D(u,v) = [(u - M/2)^2 + (v - N/2)^2]^{1/2}. \quad (5)$$

Denoting the noisy MCI by G, the denoised MCI is obtained as follows:

$$G' = \text{IFT}(\text{FT}(G) \cdot H) \quad (6)$$

where FT denotes Fourier transform, and IFT denotes inverse Fourier transform. Fig. 3 compares the MCI images before and after noise removal, and we can clearly see that the image quality is much improved, which will benefit greatly the following feature extraction and matching.

III. LINE- AND ORIENTATION-FEATURE EXTRACTION

A. Line-Feature Extraction

The principal lines and strong wrinkles are the most stable and significant features in the palmprint. In 3-D palmprint, these features are represented by high curvature regions. Therefore, it is very easy to extract the line feature from MCI by thresholding as follows:

$$L(i,j) = \begin{cases} 1, & G'(i,j) < c \cdot \mu_G \\ 0, & \text{others} \end{cases} \quad (7)$$

Fig. 4. Binarized MCI images. The white areas represent the high mean-curvature region position.

where c is a constant and μ_G is the mean value of $G'(i,j)$. We set $c = 0.7$ in the experiments by experience. Note that binary image L can be directly used for matching. Fig. 4 shows the binarized images of the MCI images in Fig. 3.

B. Orientation-Feature Extraction

The line features extracted in Section II-A can indicate where the significant structures will happen in a palm, but the orientations of these line features are not implicitly represented. Apart from the line features, the MCI also has many finer texture features, which can be well characterized by local orientations as what has been done in 2-D palmprint recognition [2]. The Gabor filters have excellent capability to extract such features. By convolving the MCI with a series of Gabor filters along different orientations, the orientation along which the Gabor filter has the greatest response can be taken as the orientation of that point. The orientation features can then be coded and matched by angular distance for identification. This process is called the CompCode scheme [2]. In this paper, the following Gabor filter is used for extracting the orientations [13]

$$\psi(x,y,\omega,\theta) = \frac{\omega}{\sqrt{2\pi}\kappa} e^{-(\omega^2/8\kappa^2)(4x'^2 + y'^2)} (e^{i\omega x'} - e^{-(\kappa^2/2)}) \quad (8)$$

where $x' = (x - x_0)\cos\theta + (y - y_0)\sin\theta$, $y' = -(x - x_0)\sin\theta + (y - y_0)\cos\theta$, (x_0, y_0) is the center of the function, θ is the orientation of the Gabor functions in radians, and $\omega = \kappa/\sigma$ is the radial frequency in radians per unit length. We set $\sigma = 4.2$ by experience, while κ is a coefficient defined by

$$\kappa = \sqrt{2\ln 2}\left(\frac{2^\alpha + 1}{2^\alpha - 1}\right) \quad (9)$$

where α is the half-amplitude bandwidth of the frequency response. Here, we choose $\alpha = 1.3785$ octave by experience. More information about Gabor filters can be found in [13]. In this paper, we set the size of Gabor filter template as 35×35 with the center position $(17, 17)$.

Based on our experiments (see Section V for details), we choose to use six Gabor filters with orientations $\theta = 0, \pi/6, 2\pi/6, 3\pi/6, 4\pi/6$, and $5\pi/6$ in the implementation for a good balance of accuracy and efficiency. Convolving the six filters with the MCI, and selecting the orientation that leads to the greatest response, we get the orientation features of MCI. Fig. 5 shows an example, from which we can see that the extracted orientations can well represent the local directional structure in a neighborhood.

IV. LINE- AND ORIENTATION-FEATURE MATCHING AND FUSION

A. Feature Matching

For the binary line-feature map, we use the AND operation to calculate the matching score between two maps. Denote by L_d the binary MCI image in the database and by L_t the input MCI image. Suppose the image size is $n \times m$. The matching score between L_d and L_t is
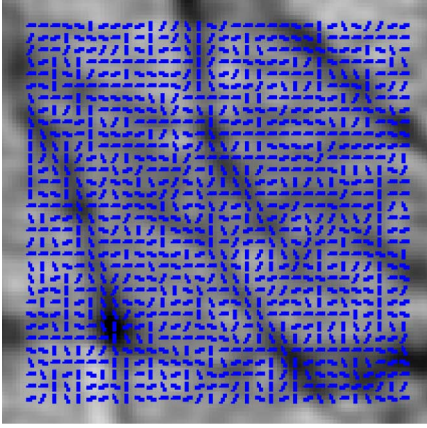
This article has been accepted for inclusion in a future issue of this journal. Content is final as presented, with the exception of pagination.

4   IEEE TRANSACTIONS ON SYSTEMS, MAN, AND CYBERNETICS—PART C: APPLICATIONS AND REVIEWS

Fig. 5.   Orientation map of an MCI.

defined as

$$R_L = \frac{2\sum_{i=1}^{n}\sum_{j=1}^{m} L_d(i,j) \oplus L_t(i,j)}{\sum_{i=1}^{n}\sum_{j=1}^{m} L_d(i,j) + \sum_{i=1}^{n}\sum_{j=1}^{m} L_t(i,j)} \quad (10)$$

where symbol "$\oplus$" means the AND logic operation. If L_d and L_t are identical, we will have the maximum matching score $R_L = 1$; on the contrary, if L_d and L_t are extremely different, the matching score will be $R_L = 0$.

For orientation features, we use integers 0–5 to code the six orientations $0, \pi/6, 2\pi/6, 3\pi/6, 4\pi/6,$ and $5\pi/6$, respectively. Intuitively, the distance between parallel orientations should be 0, while the distance between perpendicular orientations should be 3. In other cases, the distance should be 1 or 2. Let D_d and D_t be the direction sets of the MCI images. The matching score between them can be defined as

$$R_D = \frac{1}{3\,nm} \sum_{i=1}^{n}\sum_{j=1}^{m} F\left(D_d(i,j), D_t(i,j)\right) \quad (11)$$

where $F(\alpha, \beta)$ represents the angular distance between α and β

$$F(\alpha, \beta) = \min\left(|\alpha - \beta|, 6 - |\alpha - \beta|\right), \quad \alpha, \beta \in \{0,1,2,3,4,5\}. \quad (12)$$

Obviously, the value of $F(\alpha, \beta)$ can only be 0, 1, 2, or 3 as described earlier.

B. Fusion Scheme

1) Score-Level Fusion: Suppose there are n matching scores and denote them by R_i, $i = 1, 2, \ldots, n$. The commonly used score-level fusion techniques include min-score (MIN) $R_{\mathrm{MIN}} = \min(R_1, R_2, \ldots, R_n)$, max-score (MAX) $R_{\mathrm{MAX}} = \max(R_1, R_2, \ldots, R_n)$, summation (SUM) $R_{\mathrm{SUM}} = (1/n)\sum_{i=1}^{n} R_i$ and weighted average (WA) methods [14], [15]. Because the equal error rate (EER) is an important index of the matching result and it can be estimated by the training database, the weights can be determined according to the corresponding EER values. In [14], a WA scheme, called matcher weighting (MW), is proposed in the following:

$$R_{\mathrm{MW}} = \sum_{i=1}^{n} w_i R_i, \quad w_i = \frac{1/e_i}{\sum_{j=1}^{n} 1/e_j} \quad (13)$$

where w_i is the weight of R_i and e_i is the corresponding EER. The MW scheme assigns smaller weights to those features with higher EER values. Here, we adopt this fusion scheme to fuse the matching scores obtained by line and orientation features.

TABLE I
CODING OF ORIENTATION FEATURES

Orientation	Bit 1	Bit 2	Bit 3
0	0	0	0
1	0	0	1
2	0	1	1
3	1	1	1
4	1	1	0
5	1	0	0

2) Feature-Level Fusion: For line and orientation features, after coding them to bit planes, it is very convenient to combine these bit planes for matching. The six types of orientation features can be coded to 3-bits planes as illustrated in Table I [2]. The binary line-feature map can be readily represented by another bit plane (i.e., the fourth bit). Then, for each point in the MCI, we can use a 4-bits code to describe the line and orientation features. Let B_d and B_t be the 4-bits feature maps of two MCIs. The matching score between them can be efficiently calculated as follows:

$$R_f =$$

$$\frac{\sum_{k=1}^{4}\sum_{i=1}^{n}\sum_{j=1}^{m}\left((B_d^M(i,j) \cap B_t^M(i,j)) \cap (B_d^k(i,j) \otimes B_t^k(i,j))\right)}{4\sum_{i=1}^{n}\sum_{j=1}^{m}\left(B_d^M(i,j) \cap B_t^M(i,j)\right)} \quad (14)$$

where B_d^M and B_t^M are two masks, which indicate the nonpalmprint pixels, B_d^k and B_t^k represent the kth bit plane of B_d and B_t, respectively, and $\otimes$ is the bitwise exclusive OR operation.

V. EXPERIMENTAL RESULTS

In [9], a 3-D palmprint database has been established by using the 3-D palmprint imaging device developed by the Biometrics Research Center, HKPU. The database is available at http://www4.comp.polyu.edu.hk/~biometrics/2D_3D_Palmprint.htm. The PolyU 3-D palmprint database contains 8000 samples from 200 volunteers, including 136 males and 64 females between 10 and 55 years old. The 3-D palmprint samples were collected in two separated sessions, and in each session, ten samples were collected from both the left and right hands of each subject. The average time interval between the two sessions is one month. The original spatial resolution of the data is 768 × 576. After ROI extraction, the central part (256 × 256) is used for feature extraction and recognition. The z-value resolution of the data is 32 bits. In data collection, each volunteer contributed samples from both his/her right-hand palm and left-hand palm. Samples collected from the same palm belong to the same class. Therefore, there are 400 classes and each class contains 20 samples in our database.

We performed two types of experiments on the established database: verification and identification. The experiments were performed under the Visual C++ 6.0 programming environment on a PC with Windows XP Professional operation system and Pentium 4 CPU of 2.66-GHz and 1-GB RAM. In verification, the class of the input palmprint is known and each of the 3-D samples was matched with all the other 3-D samples in the database. A successful matching is called intraclass matching or genuine, if the two samples are from the same class. Otherwise, the unsuccessful matching is called interclass matching or impostor. Using the established database, there are 31 996 000 matchings in total.

In extracting the orientation features, the number of Gabor filters (see Section III-B) should be determined. To this end, we performed

TABLE II
EER BY USING DIFFERENT NUMBERS OF GABOR FILTERS TO EXTRACT THE ORIENTATION FEATURES ON 3-D PALMPRINT DATABASE

Number of Gabor filters	4	5	6	7	8	9	10	11	12
EER (%)	0.56	0.38	0.32	0.33	0.39	0.35	0.34	0.36	0.34

TABLE III
VERIFICATION PERFORMANCE AND RUNNING TIME BY DIFFERENT METHODS

|	Line feature		Orientation feature		Score level fusion		Feature level fusion		MW[9]
With BLPF	Yes	No [19]	Yes	No [19]	Yes	No [19]	Yes	No	No
Feature size (byte)	1568	1568	512	512	2080	2080	640	640	15680
EER	0.53%	0.688%	0.32%	0.495%	0.17%	0.284%	0.16%	0.268%	0.45%
Preprocessing time	1.116s	660ms	1.116s	660ms	1.116s	660ms	1.116s	660ms	660ms
Feature extraction time	96ms	96ms	97ms	97ms	183ms	183ms	182ms	182ms	125ms
Matching time	0.35 ms	0.35 ms	0.15ms	0.15ms	0.50ms	0.50ms	0.25ms	0.25ms	3.45ms
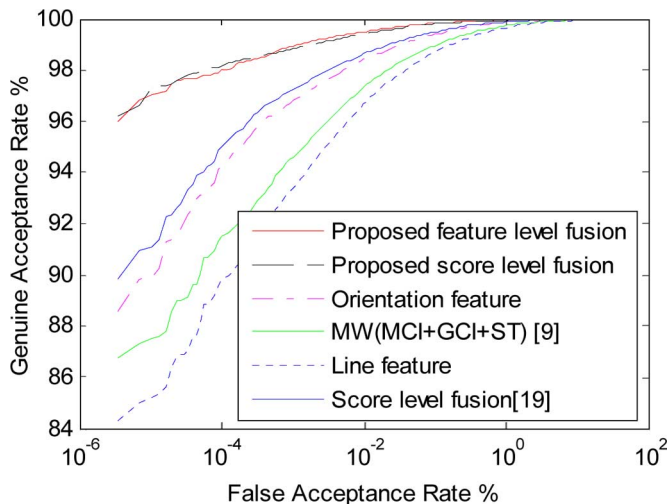
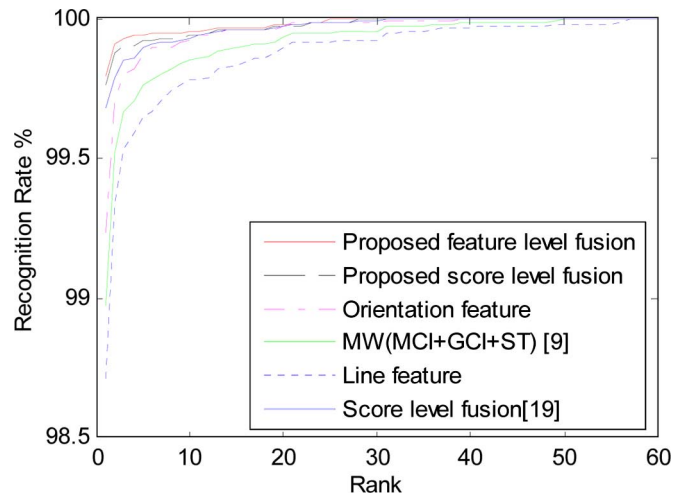Fig. 6.   ROC curves by different methods.

Fig. 7.   Cumulative match curves by different methods.

a series of experiments by using different numbers of Gabor filters to extract the orientation features on the 3-D palmprint database. The orientation θ of the Gabor filters is evenly partitioned in $[0, \pi)$. For example, if four Gabor filters are used, we have $\theta = 0$, $\pi/4$, $2\pi/4$, and $3\pi/4$. Table II lists the EER results by using 4–12 Gabor filters. We can see that the lowest EER is got by six Gabor filters. Using more than six Gabor filter cannot improve the accuracy, but increase the computational cost. Therefore, we use six Gabor filters ($\theta = 0$, $\pi/6$, $2\pi/6$, $3\pi/6$, $4\pi/6$, and $5\pi/6$) in the following experiments.

The verification experiments were performed by using each of the line and orientation features, as well as the fusion of them at score level and feature level, respectively. We compared the proposed methods with the MW method in [9], which fuses MCI, Gaussian curvature image (GCI), and surface type (ST) features on score level, and the score level fusion method in [19]. The ROC curves are shown in Fig. 6. The EER values are listed in Table III, where the feature size, the preprocessing, feature extraction, and matching time by using different features are also listed. The preprocessing in this paper includes ROI extraction and BLPF-based noise removal, while the preprocessing in [9] and [19] only includes ROI extraction. The

BLPF filtering costs about 0.5 s, but it improves the recognition accuracy significantly. From Fig. 6 and Table III, we can see that the proposed fusion methods get much lower EER than other methods. Between score-level fusion and feature-level fusion, the latter can achieve slightly better EER while requiring only half of the matching time. This implies that fusing the line and orientation features at feature level could be a more practical solution to real time 3-D palmprint identification in a relatively large-scale database.

The experiments of identification were also conducted on the 3-D palmprint database. In identification, we do not know the class of the input palmprint, but want to identify which class it belongs to. In the experiments, we let the first sample of each class in the database be template and use the other samples as probes. Therefore, there are 7600 probes and 400 templates. The probes were matched with all the templates models, and for each probe, the matching results were ordered according to the matching scores. Then, we can get the cumulative match curves as shown in Fig. 7. The cumulative matching performance, rank-one recognition rate, and lowest rank of perfect recognition (i.e., the lowest rank when the recognition rate reaches 100%) are listed in Table IV. From the experimental results, we can

TABLE IV
IDENTIFICATION PERFORMANCE BY DIFFERENT METHODS

	Line feature		Orientation feature		Score level fusion		Feature level fusion		MW [9]
With BLPF	Yes	No [19]	Yes	No [19]	Yes	No [19]	Yes	No	No
Rank-one recognition rate	98.71%	98.46%	99.24%	99.11%	99.76%	99.68%	99.79%	99.71%	98.95%
Lowest rank for perfect recognition	57	71	39	46	28	36	25	34	50

see that the performance of the proposed fusion scheme is much better than the other three methods.

VI. CONCLUSION

This paper presented simple yet efficient schemes to extract and fuse the line and orientation features of 3-D palmprint for recognition. After the 3-D palmprint image was captured, the ROI was extracted, from which the MCI was calculated. By using help to remove the high-frequency noise, we extracted the line and orientation features from MCI, which are robust features for palmprint recognition. The score level and feature-level fusion of the two types of features were proposed to match and classify the palmprints. A series of verification and identification experiments were performed on the HKPU 3-D palmprint database with 8000 samples from 200 individuals (400 palms). The experimental results showed that both the score level and feature-level fusion of line and orientation features can have much better results than using only one of them and the existing 3-D palmprint-recognition methods. Particularly, the feature-level fusion of line and orientation features can achieve better accuracy than the score-level fusion while requiring less matching time.

REFERENCES

[1] D. Zhang, A. W. K. Kong, J. You, and M. Wong, "On-line palmprint identification," *IEEE Trans. Pattern Anal. Mach. Intell.*, vol. 25, no. 9, pp. 1041–1050, Sep. 2003.

[2] A. W. K. Kong and D. Zhang, "Competitive coding scheme for palmprint verification," in *Proc. Int. Conf. Pattern Recognit.*, 2004, vol. 1, pp. 520–523.

[3] Z. N. Sun, T. N. Tan, Y. H. Wang, and S. Z. Li., "Ordinal palmprint representation for personal identification," in *Proc. IEEE Int. Conf. Comput. Vis. Pattern Recognit.*, 2005, pp. 279–284.

[4] M. G. K. Ong, T. Connie, and T. A. B. Jin, "Touch-less palm print biometrics: Novel design and implementation," *Image Vis. Comput.*, vol. 26, no. 12, pp. 1551–1560, Dec. 2008.

[5] C. Samir, A. Srivastava, and M. Daoudi, "Three-dimensional face recognition using shapes of facial curves," *IEEE Trans. Pattern Anal. Mach. Intell.*, vol. 28, no. 11, pp. 1858–1863, Nov. 2006.

[6] P. Yan and K. W. Bowyer, "Biometric recognition using 3D ear shape," *IEEE Trans. Pattern Anal. Mach. Intell.*, vol. 29, no. 8, pp. 1297–1308, Aug. 2007.

[7] V. Srinivassan and H. C. Liu, "Automated phase measuring profilometry of 3D diffuse object," *Appl. Opt.*, vol. 23, no. 18, pp. 3105–3108, 1984.

[8] H. O. Saldner and J. M. Huntley, "Temporal phase unwrapping: Application to surface profiling of discontinuous objects," *Appl. Opt.*, vol. 36, no. 13, pp. 2770–2775, 1997.

[9] D. Zhang, G. Lu, W. Li, L. Zhang, and N. Luo, "Palmprint recognition using 3-D information," *IEEE Trans. Syst., Man, Cybern. C, Appl. Rev.*, vol. 39, no. 5, pp. 505–519, Sep. 2009.

[10] W. Kühnel, *Differential Geometry: Curves-Surfaces-Manifolds.* Providence, RI: American Mathematical Society, 2006.

[11] P. J. Besl and R. C. Jain, "Segmentation through variable-order surface fitting," *IEEE Trans. Pattern Anal. Mach. Intell.*, vol. 10, no. 2, pp. 167–192, Mar. 1988.

[12] R. C. Gonzalez and R. E. Woods, *Digital Image Processing*, 2nd ed. Englewood Cliffs, NJ: Prentice Hall, 2002.

[13] T. S. Lee, "Image representation using 2D gabor wavelet," *IEEE Trans. Pattern Anal. Mach. Intell.*, vol. 18, no. 10, pp. 959–971, Oct. 1996.

[14] R. Snelick, U. Uludag, A. Mink, M. Indovina, and A. Jain, "Large-scale evaluation of multimodal biometric authentication using state-of-the-art systems," *IEEE Trans. Pattern Anal. Mach. Intell.*, vol. 27, no. 3, pp. 450–455, Mar. 2005.

[15] M. Indovina, U. Uludag, R. Snelick, A. Mink, and A. Jain, "Multimodal biometric authentication methods: A COTS approach," in *Proc. MMUA 2003, Workshop Multimodal User Authentication*, pp. 99–106.

[16] F. Li, M. K. H. Leung, and X. Z. Yu, "Palmprint matching using line features," in *Proc. ICACT 2006*, pp. 1577–1582.

[17] X. Q. Wu, D. Zhang, and K. Q. Wang, "Palm line extraction and matching for personal authentication," *IEEE Trans. Syst., Man, Cybern. A, Syst. Humans*, vol. 36, no. 5, pp. 978–987, Sep. 2006.

[18] D. S. Huang, W. Jia, and D. Zhang, "Palmprint verification based on principal lines," *Pattern Recognit.*, vol. 41, no. 4, pp. 1316–1328, Apr. 2008.

[19] W. Li, D. Zhang, and L. Zhang, "Three dimensional palmprint recognition," in *Proc. IEEE Int. Conf. Syst., Man, Cybern.*, 2009, pp. 4847–4852.